EXAMINATION OF A DNA APTAMER (TLS11a) AS A CANCER-SPECIFIC TARGETING AGENT WITHIN CULTURED BNL 1ME A.7R.1 LIVER CANCER CELLS

By

Melissa Sutton, A.S., B.S.

A thesis submitted to the Graduate Council of
Texas State University in partial fulfillment
of the requirements for the degree of
Master of Science
with a Major in Biology
December 2014

Committee Members:

Shannon Weigum, Chair

Tania Betancourt

Dana García

FAIR USE AND AUTHOR'S PERMISSION STATEMENT

Fair Use

Duplication Permission

DEDICATION

I would like to thank my family, friends, and fellow academics for all of their help and support, for not only my thesis, but for my entire collegiate career. This has been a long, arduous journey for me, and I could not have done it without the constant advice, support, and love of my mother, Elaine. She has truly been my rock for this academic adventure, never having doubts that I could fulfill my dreams of being a research scientist. My husband, Landon, has been my sanity for the past 7 years; without his steady-mindedness, calming demeanor, and love and encouragement, I would not have made it this far without having a nervous breakdown. I would also like to thank Dr. Shannon Weigum for giving me this excellent opportunity to work for her in her lab, when at times I know I was difficult to work with. Without her invitation and acceptance of "my history" I would not have a graduate degree let alone any extra experience in the field/lab. From teaching me new lab techniques to giving me real-life advice and guidance, Dr. Weigum's mentorship has truly helped me become a better scientist and person. The resounding love and support from all of my friends and family have made this dream possible for me.

ACKNOWLEDGEMENTS

The author would like to thank Mrs. Alissa Savage at the Analysis Research Service Center at Texas State University for her assistance with the confocal microscopy studies and training (NSF DBI-0821253). I would also like to thank Ms. Eugenia Barnes for her help and assistance with the nanoparticle synthesis and conjugation. Funding for this work was provided by Texas State University, the Texas Emerging Technology Fund, the Welch Foundation, and the Texas State University Graduate Thesis Research Fellowship (2014).

TABLE OF CONTENTS

Page

ACKNOWLEDGEMENTS v

LIST OF TABLES viii

LIST OF FIGURES ix

LIST OF ABBREVIATIONS x

ABSTRACT xi

CHAPTER

I. INTRODUCTION 1
- 1.1 TLS11a background and history 3
- 1.2 Polymer nanoparticles as carriers for contrast agents and chemotherapeutics (i.e. drug delivery) 8

II. MATERIALS AND METHODS 11
- 2.1 Aptamer sequences 11
- 2.2 *In vitro* cell culture 11
- 2.3 Aptamer labeling and live cell imaging 12
- 2.4 Flow cytometry analysis 13
- 2.5 Cell fractionation, SDS-PAGE, and western blots 14
- 2.6 Polymer nanoparticle synthesis, functionalization, and drug loading 16
- 2.7 MTT cytotoxicity assay 18
- 2.8 Doxorubicin drug release study 19

III. RESULTS 21
- 3.1 TLS11a aptamer labeling and localization in MEAR cells 21
- 3.2 Identification of the proteins recognized by the TLS11a aptamer 27
- 3.3 Examination of aptamer-targeted PLGA/PLA-PEG nanoparticles for drug delivery 29

IV. DISCUSSION 36

APPENDIX 39

REFERENCES/LITERATURE CITED..41

LIST OF TABLES

Table **Page**

1. Sequences of the TLS11a and TD4R aptamer 11

2. Mean fluorescent intensity obtained from flow cytometry histograms 27

3. Doxorubicin UV/Vis absorbance/fluorescence raw data 35

LIST OF FIGURES

Figure **Page**

1. Liver cancer survival statistics....2

2. TLS11a secondary structure 6

3. Confocal micrographs showing TLS11a concentration-dependent assay, 25 nM – 100 nM 22

4. TLS11a aptamer localization....24

5. Time-dependent assay with TLS11a aptamer incubation....25

6. Flow cytometry analysis of HCC cells 27

7. Fluorescent TLS11a/AlexaFluor-546 aptamer-probed western blot and SDS-PAGE gel (8 – 16% Tris-HCl) 29

8. Schematic of PLGA/PLA-PEG polymer nanoparticle synthesis....30

9. Intensity distribution of nanoparticle sizes obtained through dynamic light scattering analysis 31

10. MTT cytotoxicity assay in hepatocellular carcinoma cells....32

11. Confocal micrographs of MEAR cells treated with nanoparticle (NP) /drug conjugates 33

12. Doxorubicin fluorescence standard curve (left) and linear range at lower concentrations (right)....34

13. Release profiles for doxorubicin solution and doxorubicin nanoparticles....35

A1. TLS11a aptamer standard curve 39

A2. TLS11a aptamer standard curve linear range at lower concentrations 40

LIST OF ABBREVIATIONS

Abbreviation	Description
DMSO	Dimethyl sulfoxide
HCC	Hepatocellular carcinoma
LS	LysoSensor™ Green DND-189
PBS	Phosphate buffered saline
WGA	Wheat germ agglutinin

ABSTRACT

Hepatocellular carcinoma (HCC), the most common form of liver cancer, kills over 650,000 people worldwide every year, primarily in regions where viral hepatitis infections are common. Unfortunately, most HCC cases remain un-diagnosed until late stages of the disease when patient outcome is poor, such that death typically occurs within months to one year of initial diagnosis. In order to better care for these patients, new target-specific approaches are needed to improve early detection and therapeutic intervention. In this thesis, polymer nanoparticles functionalized with a HCC-specific aptamer were examined as potential targeted drug delivery vehicles. In particular, the *in vitro* interactions (i.e. binding and uptake) of an HCC-specific aptamer, designated TLS11a, were characterized in a hepatoma cell line via live-cell fluorescence imaging. Binding of the aptamer-AlexaFluor®546 to the cell surface was found to occur within 20 minutes of aptamer introduction. Shortly thereafter, the aptamer was taken up, presumably by endocytosis, and localized to late endosomes or lysosomes using a pH-sensitive LysoSensor™ Green dye. Next, the cell surface epitope(s) recognized by the TLS11a aptamer were characterized using SDS-PAGE and western blot procedures. A prominent band just over 21 kilodaltons (kDa) was revealed in the cell surface protein fraction, the hydrophilic fraction and in whole cell lysate but not in hydrophobic membrane fraction. Implications of this result are still being examined, but suggest that the TLS11a may recognize an extracellular peripheral membrane protein. Using a

modified nanoprecipitation technique, aptamer-functionalized polymer nanoparticles containing poly(lactic-co-glycolic acid) (PLGA) and poly(lactide)-*b*-poly(ethylene glycol) (PLA-PEG) were prepared in an organic acetone solvent then loaded with the chemotherapeutic agent, doxorubicin. Following treatment of cultured HCC cells with drug-loaded nanoparticles, there was no apparent difference in cytotoxicity between nanoparticles with or without the aptamer targeting agent; however, both nanoparticle-based treatments showed greater cytotoxicity over free doxorubicin in solution or blank nanoparticles supporting the nanoparticle itself as a viable drug delivery vehicle. Additional studies are needed to fully optimize the nanoparticle design to ensure sufficient amounts of aptamer are present on each nanoparticle and that they are readily available for molecular recognition of the target. Taken together, these preliminary studies provide support for further examination of the TLS11a as a HCC-specific targeting agent for use in polymer nanoparticle drug delivery.

CHAPTER I

Introduction

Hepatocellular carcinoma (HCC) is a highly malignant form of liver cancer which is one of the most deadly cancers in the world, killing most patients within 1 year of diagnosis.[1] HCC accounts for approximately 80% of all liver cancers with more than 30,000 new cases estimated to occur in the United States in 2014, and of those new cases nearly 22,000 will die.[1] While HCC is not very prevalent in the US, incidence rates have increased nearly 3% per year in women and 4% per year in men since 2006, primarily due to the spread of hepatitis C viral infections.[1, 2] HCC is linked to a number of pre-existing conditions such as chronic hepatitis B or C, alcohol-related cirrhosis, and nonalcoholic fatty liver disease associated with obesity, diabetes, or related metabolic disorders which are also on the rise worldwide.[1] Early detection of HCC remains challenging due to the lack of existing biomarkers with adequate sensitivity and specificity for screening high-risk patients. Even diagnostic imaging techniques, such as MRI and contrast-enhanced CT, exhibit limited sensitivity for conclusive HCC diagnosis.[3] As with many types of cancer, early detection of HCC remains the most critical determinant for patient survival. If HCC is caught early (Stage I or II), 5-year survival rates are just over 30% (Figure 1) and patients/doctors have the greatest number of treatment options including surgical resection of the tumor, nonsurgical treatment that

limits the blood supply to the primary tumor site (embolization), application of extreme heat/cold (ablation), or organ transplant.[1] Patients diagnosed with an advanced stage of HCC (Stages III & IV) exhibit 5-year survival rates as low as 2% and have far fewer choices in treatment, some of which include an organ transplant, combination chemotherapy and/or radiation therapy. Technological advances that are focused on early HCC detection, drug delivery, and even treatment selection (i.e. personalized medicine) are urgently needed to improve liver cancer patient outcomes.

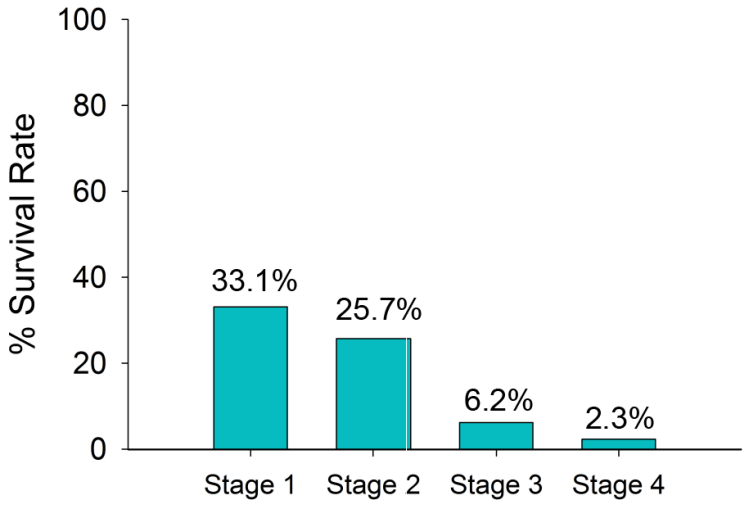

Figure 1. Liver cancer survival statistics. Five year survival rates for patients diagnosed with any form of liver cancer, including HCC, across various stages of the disease (early Stage 1 to late Stage 4). Data values are taken from the National Cancer Data Base (NCDB) American College of Surgeons Commission on Cancer.

The use of high-affinity HCC targeting agents in nanoparticle assemblies could fill this need in two ways: (i) as imaging contrast agents that localize to the tumor site and enhance optical, radiological, or magnetic detection capabilities and (ii) as targeted drug-delivery vehicles.[18] Such molecular targeted therapies have become known as theranostics because of their dual function in both diagnostics and therapy, and have been

shown to be useful for targeting cancer cells, even in the earliest stages.[6] Targeting of drugs to cancerous cells in the body and being able to visualize the interaction, almost immediately, is a paradigm shift from traditional systemic chemotherapies, with the ultimate goal being a drug that can be administered in a form such that it reaches the tumor receptor sites in sufficient concentration without doing harm (or minimal) to surrounding healthy cells, while providing a signal for site-specific detection and monitoring.[14] Examples of targeting molecules that bind cell surface proteins which have been used for early detection and targeted drug delivery include proteins, antibodies, peptides, carbohydrates and DNA aptamers.[4]

Recently, a HCC-specific aptamer (TLS11a) was described that could selectively target mouse and human hepatocellular carcinoma *in vitro*.[4] The research described in this thesis was focused on the investigation of the HCC-specific aptamer and functionalized nanoparticle conjugates for targeted labeling and drug delivery within an *in vitro* model of malignant hepatocellular carcinoma. The primary goals of the study were to (i) validate the binding and localization of the TLS11a aptamer in cultured BNL 1ME A.7R.1 cells, (ii) identify the target protein or epitope recognized by the aptamer and (iii) examine the efficacy of aptamer-targeted PLA-PEG nanoparticles for doxorubicin drug delivery.

1.1 TLS11a aptamer background and history

Aptamers are short (approximately 50-100 nucleotides in length), single-stranded oligonucleotides made of DNA, RNA, or modified (XNA) nucleic acids that have been chosen via the SELEX *in vitro* process from a DNA/RNA/XNA library for their specific recognition of a selected target, or ligand, such as HCC cells/tumors.[5,6] The SELEX

process, or systematic evolution of ligands by exponential enrichment, combines a large group of oligonucleotide sequences (~10^{12} - 10^{15}) with a known target molecule; any sequences that are bound to this molecule are kept and then amplified via PCR/RT-PCR and *in vitro* transcription.[19] The amplified sequences are then put through additional cycles of amplification both with the prior target molecule and a non-target molecule. After each cycle, the sequences with affinity for the target molecule are kept and those with affinity for the non-target cell are rejected, thereby enriching the population in oligonucleotides that differentiate between target and non-target.[19] Enriched pools of sequences are then cloned and the positive clones are sequenced to identify individual aptamers.[19] Ligands may include small molecules, peptides, proteins, whole cells, tissues or even organisms.[5,6] Benefits to using these high-affinity ligands over antibodies include how inexpensive aptamers are to make, aptamers can be synthesized in large quantities, functionalized for numerous applications, and they have a relatively long shelf life.[9] Aptamers are able to fold into complex three-dimensional structures with distinct molecular binding patterns.[18] This increased functionality, over antibodies, enables attachment to other biomolecules or solid surfaces using a variety of conjugation chemistries and can facilitate the detection or tracking of the aptamer either *in vitro* or *in vivo.*[7, 8]

The TLS11a aptamer (Figure 2) was first described by the Tan group[4] from the University of Florida, where they used a modified whole-cell SELEX procedure involving two different liver cell lines, one for the target cell line and the other as a negative control for counter selection—the BNL 1ME A.7R.1 (MEAR) mouse liver cancer cell line and its normal liver cell line counterpart BNL CL.2 (BNL), respectively.

The cell lines were selected due to their similarity in morphology and their ability, or lack thereof, to form tumors. After 16 rounds of selection from a ssDNA pool of approximately 200 pmol, the selected sequences were amplified through PCR using unmodified primers and cloned into *Escherichia coli*, after which they determined the sequence using their onsite Genome Sequencing Services Laboratory.[4] Enrichment and selectivity was monitored via flow cytometry (for suspended cells) and fluorescence confocal imaging (for adherent cells) throughout the entire selection process. Aptamer characterization studies of TLS11a were shown to have a high binding affinity for mouse HCC cells *in vitro* using the BNL 1ME A.7R.1 (MEAR) cell line with a reported K_d = 4.5±0.4nM.[4] Specificity for HCC was established against various cell lines including normal mouse liver, normal/malignant mouse liver tissue sections, and a human liver cancer cell line.[4] The TLS11a aptamer was found to bind to not only MEAR cells, but also the human liver cancer line Huh7 and to a lesser extent human lung cancer line, H23; however, the probe sequence did not bind to any cells in normal liver tissue or in any suspended cell lines like leukemia and lymphoma.[4] Their research showed that TLS11a exhibited a strong binding affinity for adherent, solid tumor cells, and could prove beneficial for determining possible biomarkers for the detection of cancerous cells; although, the target surface protein/epitope on the tumor cells remains unknown.

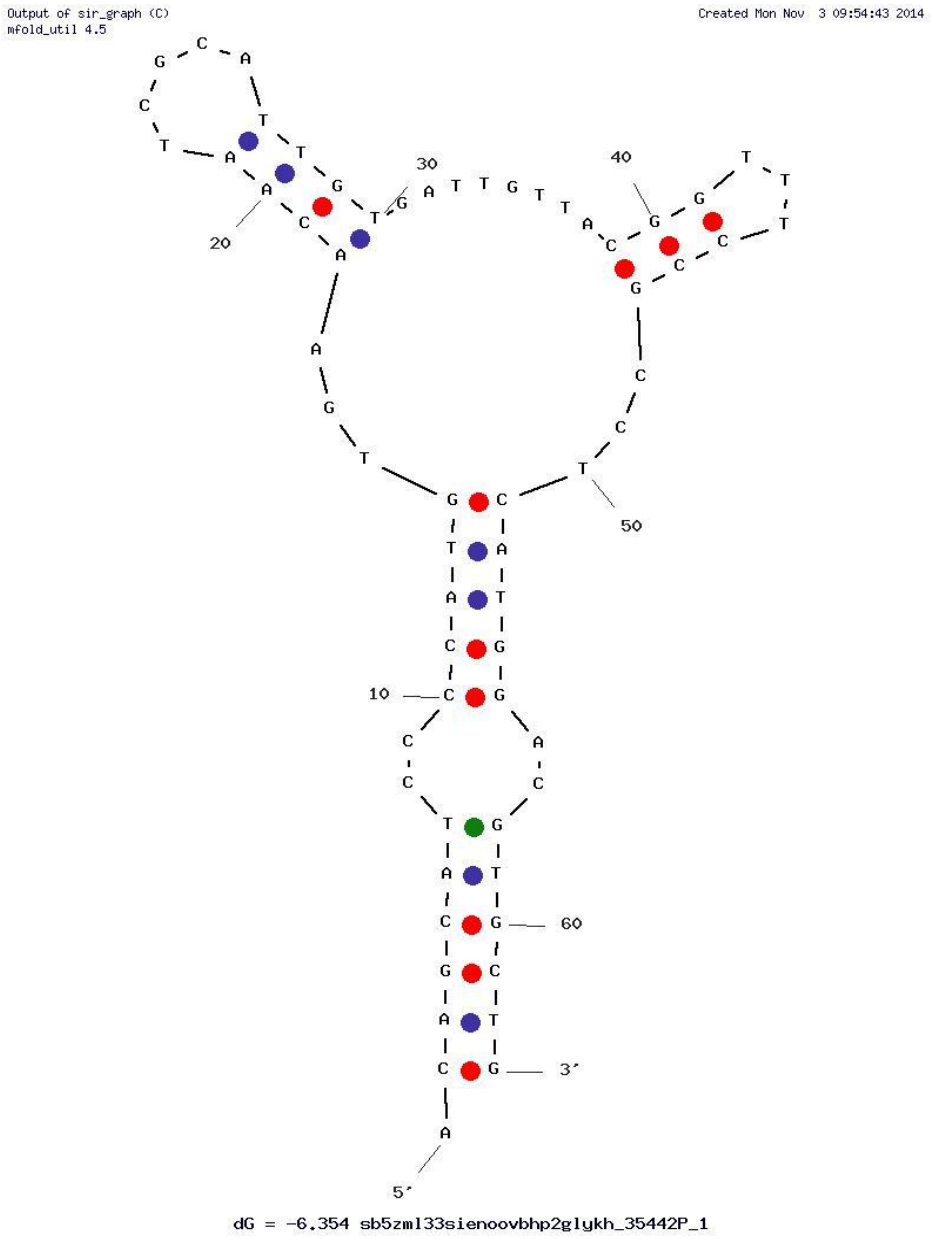

Figure 2. TLS11a secondary structure. Image generated using idtdna.com sequence generator for ~39°C; ΔG = -6.35 kcal/mole and ΔH = -142.1 kcal/mole.

The Tan group has explored utility of the TLS11a aptamer in targeted drug delivery using a modified aptamer sequence containing a long 5'-GC tail, referred to as TLS11a-GC, that intercalates the chemotherapeutic agent, doxorubicin (TLS11a-GC-Dox).[9] Doxorubicin is an anthracycline antibiotic that prevents DNA synthesis and transcription by intercalation between DNA nucelotides.[18] The doxorubicin molecule is comprised of flat, aromatic ring structures that preferentially bind to double-stranded 5'-GC-3' sequence; TLS11a is comprised of two of these sequences.[9] Each 5'-GC-3' sequence is capable of intercalating two doxorubicin molecules, therefore the modified aptamer dimer structure with a 5'GC tail extension used by Tan et al. was capable of intercalating up to 28 doxorubicin molecules per aptamer sequence at a TLS11a-GC-to-doxorubicin ratio of 1:25 (TLS11a modified sequence, 5'-CGCGCGCGCGCGCGCGCGCGCGCGCGCGCGCGCGCGCGCGCGCGCGCGCGCGCGACAGCATCCCCATGTGAACAATCGCATTGTGATTGTTACGGTTTCCGCCTCATGGACGTGCTG-3').[9] Previous studies from Zhang et al. have shown that intercalation of doxorubicin into a known RNA aptamer sequence, A10, (A10 aptamer to doxorubicin ratio of 1:1.1) had explicit apoptotic efficacy against prostate cancer cells.[29] The addition of a long GC tail was intended to maximize the intercalation capacity of the chemotherapeutic agent, doxorubicin.[9] To confirm the attachment by this aptamer to the cell's surface, a protease assay was performed to determine membrane protein binding efficiency.[9] This assay included the testing of a human liver cancer cell line, LH86, where cells were treated with trypsin for 10 minutes at physiological temperatures and conditions, followed by two ice-cold PBS washes via centrifugation and resuspension, then incubated with the fluorescently labeled TLS11a aptamer.[9] They found that the

fluorescence signal was reduced to background levels, suggesting the protease-treated cells that underwent surface protein digestion lacked the target membrane protein/epitope for the aptamer, hence the lack of signal.[9] Importantly, this result suggested that the molecule targeted by this aptamer is a membrane-bound protein. However, there was no therapeutic benefit over free doxorubicin *in vitro* and only a modest decline in mouse HCC tumor volume was reported *in vivo.*[9] This limited effect was attributed to kinetic differences between uptake mechanisms of the aptamer conjugate, likely through endocytosis, versus the membrane-diffusible free doxorubicin.[9]

1.2 Polymer nanoparticles as carriers for contrast agents and chemotherapeutics (i.e. drug delivery)

Chemotherapeutic drugs encapsulated in the matrix of polymer nanoparticles like PLGA, or poly(lactic-co-glycolic acid), are commonly used as drug delivery vehicles, vaccines, and biological macromolecules due to their rapid internalization and release from the endo-lysosomes.[10] PLGA, PLA and PEG are biocompatible polymers that have been approved by the FDA for use in various drug-delivery systems.[10] The PLGA copolymer is degradable in water, and therefore the body; through the process of hydrolysis, PLGA is broken down into the original monomers, lactic acid and glycolic acid. These monomers are natural by-products of numerous metabolic pathways performed in the human body, resulting in limited cytotoxicity. Cellular uptake of polymer nanocarriers can vary based upon their size, shape, flexibility, surface charge, as well as their chemical composition.[11] Many applications using polymer nanoparticles have shown great potential due to the enhanced permeability of tumors, which permits passive targeting.[13] This passive effect of nanoparticles, which are preferentially retained

by tumors, allows for the passing of 10 – 500 nm drug delivery vehicles to tumors with their own blood supply.[13] In contrast, chemotherapeutic agents not having been conjugated or trapped to a nanoparticle or aptamer, like doxorubicin, are generally toxic to healthy cells.[13] Packaging this drug into a nanoparticle and conjugating it to a high-affinity binding aptamer would ideally improve the binding specificity of this drug delivery molecule to its target cell, avoiding the surrounding healthy/normal cells.[25]

Yu et al. synthesized paclitaxel-loaded PLGA nanoparticles via the emulsion/evaporation technique, with S2.2 aptamer conjugation occurring at the particles' surface through a DNA spacer resulting in nanoparticles approximately 225.3 nm in diameter.[25] The S2.2 aptamer is specific for the over-expressed MUC1 protein found on the surface of MCF-7 cells, a human breast cancer line; they used a MUC1-negative hepatic cancer cell line, HepG2, as their control.[25] Flow cytometry results confirmed an increase in cellular binding by the S2.2 aptamer to target cells with enhanced cytotoxicity to these same cancer cells with the MUC1 surface protein, compared to those cells lacking the over-expressed surface protein (HepG2).[25] Further analysis with the spacer modified aptamer S2.2-spacer showed similar results in that there was no decrease in surface binding to cells having the MUC1 protein suggesting the maintained selective binding ability of the original aptamer sequence.[25] The S2.2-spacer aptamer was then conjugated to nanoparticles after activation by EDC and NHS reaction chemistry. EDC, or 1-ethyl-3(-3-dimethlyaminopropyl)carbodiimide, is a water soluble compound used to activate the carboxyl terminal on the end of the PLA-PEG-COOH monomer. This chemical process resulted in amine-reactive N-hydroxysuccinimide esters cross-linking with the primary amine on the 5' end of the TLS11a aptamer forming an

amide bond between the aptamer and polymer. MUC1-positive and MUC1-negative cells were incubated with nanoparticles and nanoparticles with the modified aptamer-spacer, and results show an increase in cellular binding and uptake by nanoparticle-aptamer conjugates when compared to results with MUC1-negative cells.[25] To further validate this drug delivery complex, a cytotoxicity study was performed using various complexes incubated with both cell lines, MCF-7 and HepG2—complexes included free paclitaxel (known to be cytotoxic to cells), paclitaxel-loaded nanoparticles without aptamer probe, paclitaxel-loaded NPs conjugated to both a random aptamer sequence and the MUC1-positive aptamer (S2.2), and plain/blank nanoparticles.[25] The paclitaxel was found to be cytotoxic to both cell lines, as was expected. The paclitaxel-loaded nanoparticles exhibited signs of cytotoxicity though not as much as the paclitaxel-nanoparticle-aptamer conjugates which presented the highest cytotoxicity in the MCF-7 cells, and exhibited little to no cytotoxicity to the HepG2 cells with all viability remaining near 100%, suggesting the S2.2 aptamer could selectively enhance the drug delivery to MUC1-positive cells.[25]

In this thesis, the TLS11a HCC-specific aptamer was used as a targeting agent on the surface of PLGA/PLA-PEG nanoparticles in order to better understand the binding and uptake of aptamer-targeted polymer nanoparticles within the HCC *in vitro* model system employed by Meng et.al.[9] The interaction of these nanoparticles, once incorporated with a drug, was evaluated using a MTT assay and fluorescent microscopy. Western blot analysis was employed to identify the surface protein responsible for aptamer attachment and binding.

CHAPTER II

Materials and Methods

2.1 Aptamer sequences

The TLS11a HCC-specific aptamer and TD4R aptamer, sequences listed in Table 1, were purchased from Integrated DNA Technologies (IDT; Coralville, Iowa) with an Alexa-Fluor®546 fluorophore (556 nm excitation/573 nm emission maxima) attached to the 5' terminal end. All aptamers were purified using high pressure liquid chromatography and resuspended at a stock concentration of 100 µM in Tris/EDTA buffer (pH 8.0; AM9858, Ambion® Life Technologies). TLS11a is a hepatocellular carcinoma-specific aptamer, where TD4R is the negative control. Both aptamers are comparable in length and GC content in an effort to maintain comparable thermal stability between the two sequences.

Table 1. Sequences of the TLS11a and TD4R aptamer.

Aptamer	Target	Length	Sequence
TLS11a	Hepatocellular carcinoma	63 nucleotides	5' – ACAGCATCCCCATGTGAACAATCGCATTGTGATTGTTAC GGTTTCCGCCTCATGGACGTGCTG – 3'
TD4R	Negative control	63 nucleotides	5' – ATCCGTCACACCTGCTCTTGACACGCGTACGGGTCC GGACATGTCATAACGGACTGGTGTTGG – 3'

2.2 *In vitro* cell culture

The mouse BNL 1ME A.7R liver hepatoma cell line, also referred to as MEAR cells (ATCC® TIB-75™), was grown in cell culture at 37°C and 5% CO_2 in a complete growth medium consisting of a 500 ml 1:1 mixture of Dulbecco's Minimum Essential Medium (DMEM)/ F-12 media (D6421; Sigma). Additional supplements added to the DMEM include 10% fetal bovine serum, 200 mM L-glutamine (G2150; Hybri-Max®

Sigma), and 100 U/ml penicillin-streptomycin (ATCC #30-2300). Cells were seeded into T-25/T-75 culture flasks for growth and splitting, into Lab-Tek™ II four-chambered slides (Thermo Scientific) for microscopy studies, and round Delta-T® culture dishes (Bioptechs Inc.) for use with the heated stage adaptor on the confocal microscope. Seeding densities remained constant for all assays and microscopy studies at 1 x 10^4 cells/cm^2. Upon reaching ~80% confluency, the cells were stained for imaging/analysis, subcultured into a new culture vessel, or frozen for future use.

2.3 Aptamer labeling and live cell imaging

Approximately 24 hours after seeding in Delta-T® dishes, MEAR cells were incubated with the TLS11a or negative control aptamer (TD4R) at 37°C and 5% CO_2 for up to 60 minutes with a final concentration range of 25 – 100 nM in DMEM. Cell nuclei were stained by adding 2 drops/ml media NucBlue® Live Cell Stain (R37605; Molecular Probes® Life Technologies) for the final 20 minutes of the aptamer incubation period. Following incubation, the culture medium was removed and the cells were washed three times with warm phosphate buffered saline (PBS; BupH Dry Buffer Pack #28374, Pierce/Thermo Scientific). Fresh DMEM/F-12 media was added for live-cell confocal imaging, performed using a Delta-T® Open Dish System (Bioptechs Inc.) with heated stage adapter on an Olympus FluoView FV1000 laser scanning confocal microscope.

For the cellular uptake and localization studies, cells were labeled with the aptamer, an Alexa-Fluor®647 conjugated wheat germ agglutinin (WGA)(650 nm excitation/668 nm emission) and a pH-sensitive LysoSensor™ Green DND-189 (443 nm excitation/505 nm emission, pK_a 5.2; Molecular Probes® Life Technologies) according to manufacturer's protocol. WGA contains a group of closely related isolectins, for which

the receptor sugar for is *N*-acetylglucosamine, with preferential binding to dimers and trimers of this sugar and has also been reported to interact with some glycoproteins via sialic acid residues on cell surface glycoproteins/glycolipids. In viable cells, WGA acts as a cell surface membrane marker due to its impermeant nature while the LysoSensor™ dye was used to stain late endosomes and lysosomes. The LysoSensor™ was added for the final 30 minutes of the aptamer incubation at a final concentration of 3µM in DMEM/F-12 media, followed by NucBlue® and WGA for the remaining 4 minutes of aptamer incubation at 1 µg/ml in DMEM/F-12, all at 37°C in 5% CO_2 incubator. Following incubation, cells were washed with and imaged as described above.

2.4 Flow cytometry analysis

MEAR cells were grown in T-25/T-75 flasks until reaching ~80% confluency and were then treated with trypsin (TrypLE™ Express, Gibco® Life Technologies) for 8 minutes at 37°C to detach the cells from the flask bottom. Cells were washed twice with PBSA and centrifuged at 3,000rpm for 5 minutes to remove any remaining phenol-red DMEM medium or trypsin. After washing, the cell pellet was resuspended in PBSA and counted using a hemacytometer. The staining protocol included taking 1 x 10^6 total cells and incubating that suspension in 90 µl PBSA with 10 µl of TLS11a and TD4R, at a final aptamer concentration of 5 µM, for 1 hour at 4°C with brief mixing at approximately 15 minute intervals. Following incubation, the cells were washed twice with PBS and kept on ice until ready for analysis. Samples were analyzed on a microfluidic chip-based Sony SH800 Flow Cytometer and included unstained MEAR cells (negative control) and cells that were incubated with both the TLS11a and TD4R aptamers. Initial gating parameters were set to include data from the front scatter and back scatter of selected cells, followed

by a parameter quantifying the front scatter area versus the front scatter height eliminating any doublet cells outlying in the histograms. For each gated cell population, 10,000 total events were measured and collected.

2.5 Cell fractionation, SDS-PAGE, and western blots

Cell surface proteins were biotinylated, extracted and purified using the Pierce Cell Surface Protein Kit (#89881; Thermo Scientific) according to the manufacturer's protocol. This involved biotinylation of surface proteins in viable, attached MEAR cells followed by cell dissociation (cells removed from flask surface using a scraping tool) and mechanical lysis via sonication, while on ice. Biotinylated proteins were extracted using the supplied streptavidin affinity column, and eluted into 2X Laemlli sample buffer (Bio-Rad) with 50 mM dithiothrieotol (DTT), a strong reducing agent; prior to SDS-PAGE gel loading the samples were boiled at 100°C for 5 minutes. Using a phase separation-based technique via the FOCUS™ Membrane Protein Fractionation Kit (G Biosciences®), cell membrane proteins were isolated from MEAR cells, per manufacturer's protocol. Quantification of the collected membrane protein fractions, and whole cell lysates, was established using an A_{280}/A_{260} assay resulting in total protein concentration. One hundred microliters of the hydrophilic and hydrophobic protein extracts were cleaned up with the Pierce SDS-PAGE Sample Prep Kit (#89888; Thermo Scientific) then diluted in 5X sample buffer[12] and boiled at 100°C for 5 minutes. Quantification of total protein from the cell surface membrane protein fraction could not be performed due to the sample being eluted in 5X sample buffer during the prep protocol, per manufacturer's instructions. Determining the protein concentration for this cell surface membrane fraction was done by starting with a known cell membrane protein concentration and

using the same final volume of cell surface protein fraction and then comparing their band distribution after electrophoresis. A couple of gels were run, maintaining the protein concentration of the total cell membrane proteins and adjusting the volume of cell surface membrane proteins until the bands were comparable. The sample volumes were then adjusted until there was 10-25 µg of total protein in each of 8 wells in the 8-16% Mini-PROTEAN® TGX™ pre-cast gradient gel (Bio-Rad). Gels were run at 200V until the bands were ~1 cm from the bottom of the gel, then one gel was transferred onto a nitrocellulose membrane at 100V for 1 hour, while the other was stained in a Coomassie blue solution.[12] After the transfer, the nitrocellulose membrane was curled so that it fit in a 50 ml conical tube; it was necessary to trim the edges to prevent the membrane surfaces from overlapping. First, the membrane was washed three times in a wash buffer containing 0.5% bovine serum albumin and 0.01 µg/ml tRNA (Sigma; R5636) at room temperature for 5 minutes each wash step, while rotating. After the third wash step, the wash buffer was removed and a blocking buffer containing 3% PBSA and 0.1 µg/ml tRNA (to reduce non-specific binding) was added to the tube and was rotated at room temperature for one hour. Once the membrane had been blocked, it was rinsed 3 times in the same wash buffer as previously mentioned, then probed with 1 nM TLS11a aptamer/Alexa-Fluor®546 in wash buffer overnight, while rotating at 4°C. The next morning, the membrane is washed a final time with wash buffer and then allowed to air dry at room temperature, while being protected from light. The fluorescently probed membrane was imaged on a Pharos FX™ Plus Molecular Imager (Bio-Rad) with suitable fluorescence filters.

2.6 Polymer nanoparticle synthesis, functionalization, and drug loading

The PLGA, or poly(lactic-co-glycolic acid) used for the nanoparticle preparation was obtained from LakeShore Biomaterials. The monomers PLA-mPEG, or poly(lactic acid)-*b*-poly(ethylene glycol), with a methoxy end group, and PLA-PEG-COOH, or poly(lactic acid)-*b*-poly(ethylene glycol), were synthesized through the aromatic ring-opening polymerization of lactide dimers onto the carboxyl terminal end of the PLA-PEG-COOH compound, as previously described in section 1.2 above.[13] PLGA is a copolymer complex made by polymerizing the monomers lactic acid and glycolic acid with ester linkages, resulting in an aliphatic (non-aromatic) polyester compound.

Polymer nanoparticles were prepared using a modified nanoprecipitation method.[13, 14] Briefly, the organic phase consisted of a polymer solution and a mixture of organic solvents, in this case 1.5 mg of PLGA, 0.75 mg of PLA-mPEG, and 0.75 mg of PLA-PEG-COOH were dissolved in acetone (2:1:1 mass ratio of PLGA/PLA-mPEG/PLA-PEG-COOH), resulting in a final polymer concentration of 30 mg/ml. A volume of 100 μl of this organic solution was added drop-wise to 2 ml of an aqueous solution (diH_2O) while stirring. For nanoparticles containing doxorubicin, a doxorubicin concentration of 1.667 mg/ml in methanol (82:18 volume ratio of acetone to methanol) was added to the copolymer solution to achieve a 1% w/w target loading of doxorubicin in the nanoparticles. All nanoparticles were washed two times via centrifugation, with resuspension in fresh deionized water, to remove any unencapsulated drug and excess stabilizer remaining in solution. Blank nanoparticles were prepared similarly, except that pure methanol replaced the doxorubicin solution for a drug-free nanoparticle complex.

To attach the aptamers to the surface of the nanoparticles, carbodiimide chemistry was used to activate the terminal carboxylic acids of PLA-PEG-COOH into amine-reactive N-hydroxysuccinimide esters. For this purpose, the nanoparticles were resuspended in MES buffer, or 2-(*N*-morpholino)ethanesulfonic acid, pH 6.0, and reacted with EDC, or 1-ethyl-3-(3-dimethylaminopropyl)carbodiimide and NHS, or *N*-hydroxysuccinimide for 15 minutes (50-fold molar excess of EDC and NHS to carboxylic acids groups of the PLA-PEG-COOH copolymer). The pH of the suspension was brought up to 7.4 by addition of 2X phosphate buffered saline (PBS). For aptamer attachment, 5 µl of both the TLS11a and TD4R aptamers, or an equal volume of PBS for the particles without aptamer conjugates, was added to the nanoparticle solution and allowed to react at room temperature for 4 hours while protected from light. After the reaction was complete, hydroxylamine was added to quench any excess EDC and activated carboxylic acids. The nanoparticles were then washed via centrifugation with deionized water to remove excess reagents and unbound aptamer molecules leftover from the reaction chemistry. The nanoparticles were finally resuspended in fresh PBS for immediate use with cellular studies.

Nanoparticle size was characterized by dynamic light scattering using a Malvern ZetaSizer Nano ZS instrument. Doxorubicin concentration was determined using fluorescence spectroscopy. For this study, the concentration of the drug in nanoparticle suspensions was determined from the intensity profile of the absorption (488 nm) and emission (595 nm) peaks of the suspensions with a standard calibration curve.

2.7 MTT cytotoxicity assay

Eight duplicate batches of doxorubicin-loaded nanoparticles, both with and without aptamer functionalization, were serially diluted in DMEM/F-12 growth media with final doxorubicin concentrations of 500 nM, 250 nM, 125 nM, 62.5 nM, 31.3 nM, 15.6 nM, 7.8 nM and 3.9 nM, respectively. Control batches included equal volumes of blank nanoparticles (no aptamer or doxorubicin) and free doxorubicin at the same concentrations. MEAR cells were seeded into 96-well plates at a seeding density of 5,000 cells/well and allowed to adhere to the surface (~24 hours after seeding) before treating them with the nanoparticle/media suspensions and incubating them for 72 hours at 37℃ in 5% CO_2. Once the 72 hours was up, the medium containing the treatment solutions was removed and MTT reagent (3-(4,5-dimethylthiazol-2-yl)-2,5-diphenyltetrazolium bromide) prepared in phenol red-free media at 0.05 mg/ml was added to each well and incubated at 37°C in 5% CO_2 for up to 4 hrs.

Medium was removed from the wells and 100 µl of dimethyl sulfoxide (DMSO) was added to each well and the plates were placed on a microplate shaker until the crystals dissolved. Each plate had its absorbance read at 555 nm and 700 nm wavelengths using the BioTek™ Synergy H1 Hybrid Multi-Mode Microplate Reader and resulting data was graphed in SigmaPlot™ version 12.5 (Systat Software, Inc.) utilizing a four-parameter logistic function for the best fit regression line. Imaging studies involved incubating adherent MEAR cells grown in chambered slides with the nanoparticle/drug solutions at 500 nM in DMEM/F-12 growth media 37°C in 5% CO_2 for 2 hours, after which the cells were rinsed with PBS and fixed in ice-cold methanol for 15 minutes, air dried and cover slip mounted with 90% glycerol, all while being protected from light.

2.8 Doxorubicin drug release study

Drug release study was performed *in vitro* using 10 mM PBS (Thermo Scientific, Cat#: 28374). For the purpose of this study, three different samples, all in triplicate, were made using (i) blank nanoparticles (no drug), (ii) doxorubicin-loaded nanoparticles, and (iii) a free doxorubicin solution, yielding nine total samples. To ensure the concentration of doxorubicin in the nanoparticles matched that of the free doxorubicin, for comparison, 100 µl of nanoparticle-doxorubicin suspension was placed into a black 96-well plate and the absorbance was read from 300 nm – 800 nm with 1 nm increments; fluorescence was measured at 500 nm – 800 nm (doxorubicin's maximal excitation is wavelength is 480 nm). The 1.667 mg/ml stock doxorubicin solution was progressively diluted with PBS until the absorbance spectra matched that of the doxorubicin-loaded nanoparticles, resulting in a 65.2 µg/ml solution. Nine 50 ml Falcon tubes with 10 ml warm PBS were placed into a 37°C water bath. Additionally, nine Tube-O-Dialyzer (G-Biosciences, 786-618) tubes were rinsed with deionized water before having 250 µl of each above mentioned sample added to their conical reservoir. Tubes were turned upside down, and flicked with my finger so that the samples were in contact with the dialyzer tube's permeable membrane; parafilm was placed over top of the opposite end so that condensation would not get inside the hollow tube after inversion. Tubes were then placed into the Falcon tubes, membrane-side down, in the PBS solution, protected from light and placed into the pre-heated 37°C hot water bath. At pre-determined time points, 500 µl samples were taken from each of Falcon tube, from the surrounding PBS solution; after collection, 500 µl of warm, fresh PBS was added back to each tube. Time points included hours 1, 2, 3, 6, 9, 12, 18, 24, 30, 36, 48, 60, 72, 96, and 120, and samples

collected were stored in 4°C, protected from light, until ready for analysis. Analysis included loading a 96-well plate with 100 µl samples of each replicate and reading the absorbance at 480 nm, and the fluorescence at 480 nm excitation/590 nm emission, respectively. A standard curve for doxorubicin was created to deduce the concentration of the drug at each wavelength (appendix, Figure 2).

CHAPTER III

Results

3.1 TLS11a aptamer labeling and localization in MEAR cells

Initial *in vitro* labeling experiments were conducted in order to determine the optimal concentration of TLS11a/Alexa-Fluor®546 and verify its specificity relative to an irrelevant aptamer control. Following a 60 minute incubation with the aptamer at concentrations ranging from 0-100 nM, fluorescent labeling intensity was found to increase in a concentration-dependent manner from 25 nM up to 100 nM (Figure 3, right column). The irrelevant control aptamer of similar length and GC content exhibited very low binding and fluorescence labeling intensity at these same concentrations (Figure 3, left column).

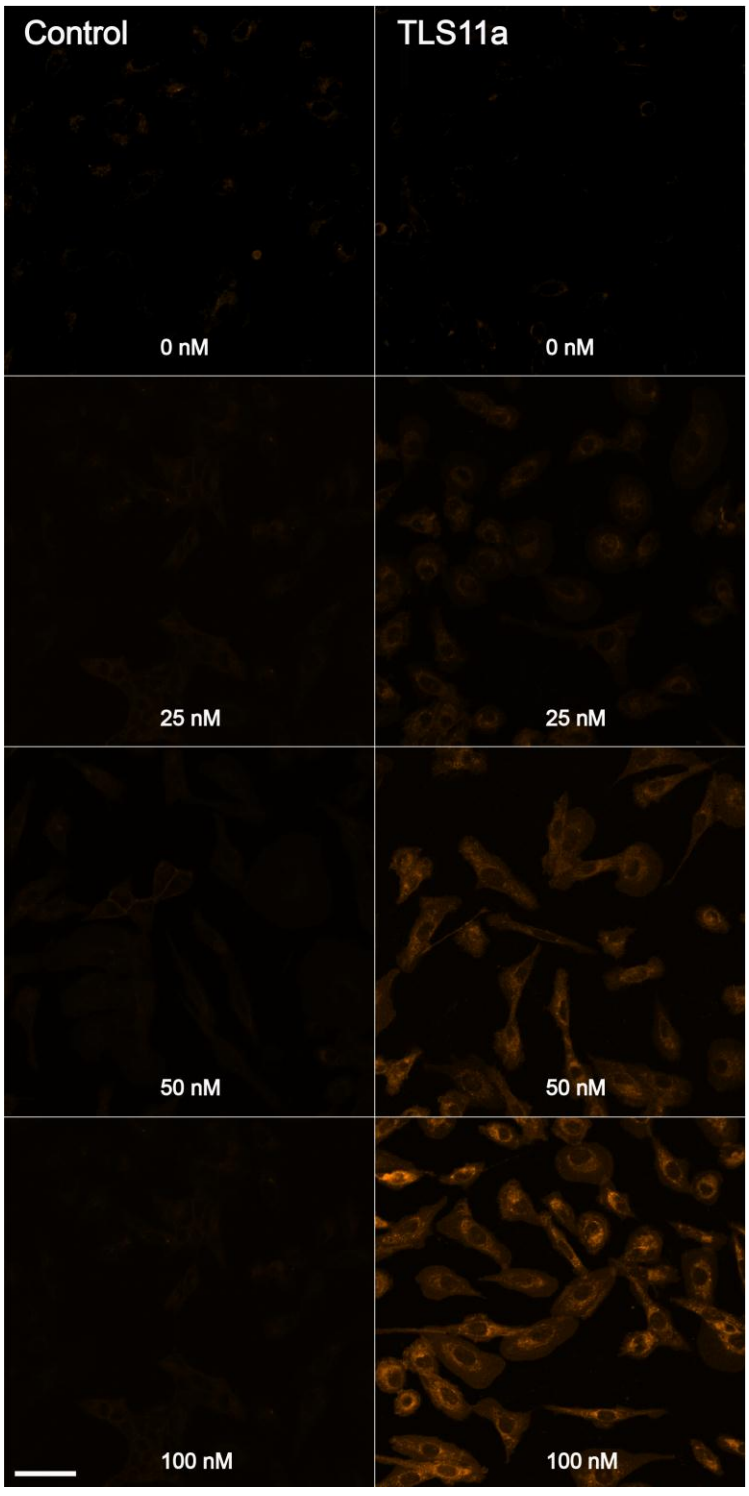

Figure 3. Confocal micrographs showing TLS11a concentration-dependent assay, 25 nM – 100 nM. Confocal micrographs (z-projections) of mouse hepatoma (MEAR) cells labeled with Alexa-Fluor®546 conjugated TLS11a aptamer (right column) versus an irrelevant negative control aptamer TD4R/Alexa-Fluor®546 (left column) at increasing concentrations. Micrographs were obtained using a 20x/0.95 numerical aperture water immersion objective at a z-step size of 1.0 µm. Scale bar is 20µm.

The localization and uptake of the TLS11a aptamer was examined through live-cell imaging of triple labeled MEAR cells that were treated concurrently with the aptamer, a pH sensitive lysosomal dye, and a cell membrane marker. A representative confocal single optical selection from the 60 minute treatment set is shown in Figure 4. Cellular structures labeled by the TLS11a aptamer (orange channel) were also stained strongly with the WGA/AlexaFluor-647 cell membrane marker (red channel) which suggested a large degree of aptamer binding at the cell surface (Figure 4). In addition, the aptamer was found to localize to discrete spherical structures brightly stained with the LysoSensor dye (Figure 4, green channel arrow) indicative of acidic compartments in the endo/lysosomal pathway. These results suggest that the TLS11a aptamer is capable of binding at the cell surface and being taken up into the cells, two essential criteria of a high-affinity targeting ligand for use in drug delivery. In time-dependent experiments, the TLS11a aptamer labeling at the cell surface appeared within 20 minutes of aptamer treatment while lysosomal localization began 30 minutes post-treatment, reaching a maximum at roughly one hour (Figure 5).

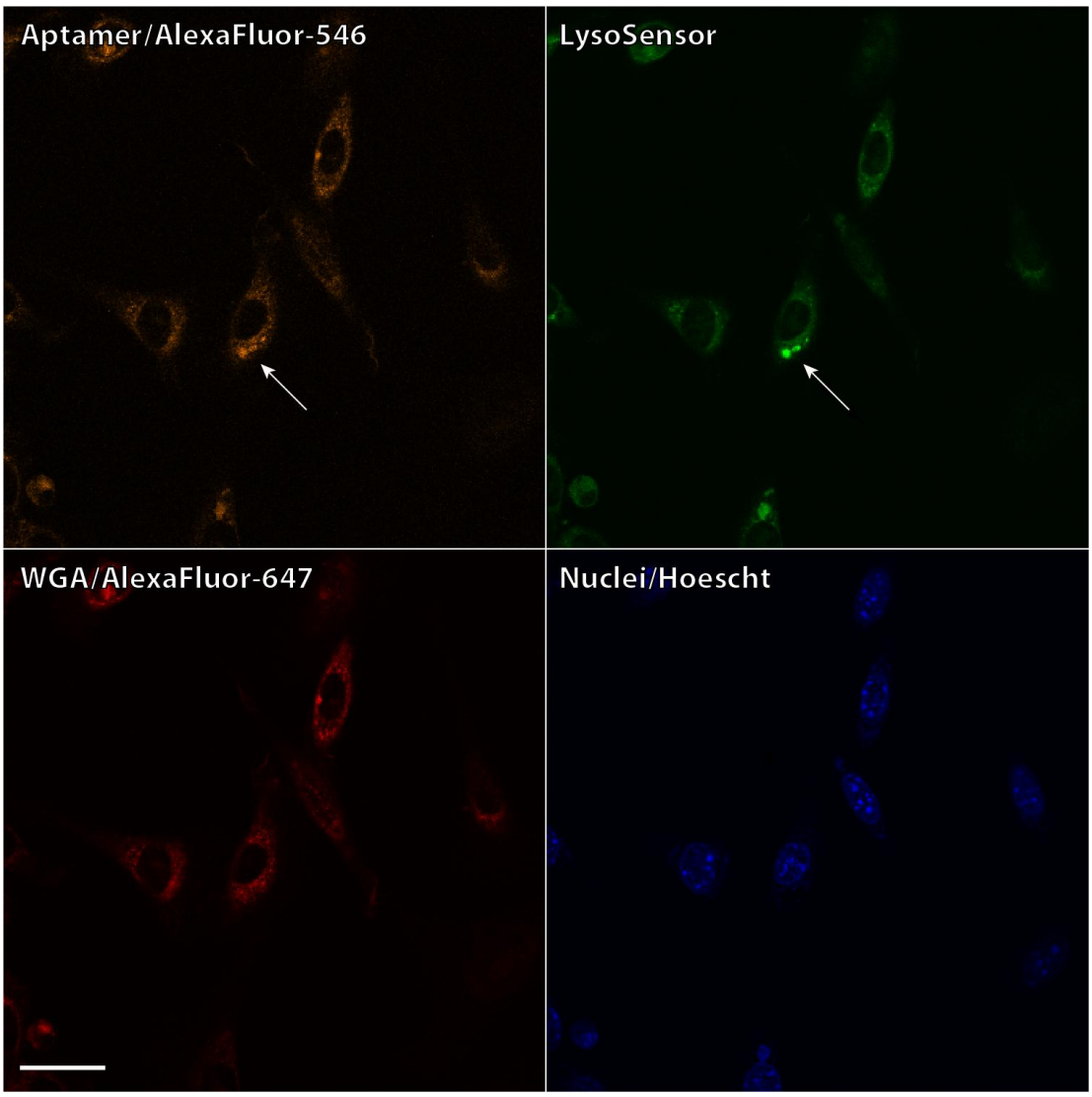

Figure 4. TLS11a aptamer localization. Confocal z-slice of live hepatocellular carcinoma (MEAR) cells labeled with a Hoescht nuclear membrane marker (blue), TLS11a/AlexaFluor-546 aptamer (orange), a pH sensitive lysosomal marker (green) and a cell membrane marker (red). Localization of the TLS11a aptamer to late endosomes or lysosomes is shown with a white arrow. All micrographs were obtained using 60x/1.0 numerical aperture water immersion objective at a z-step size of 1.0 µm. Scale bar is 10 µm.

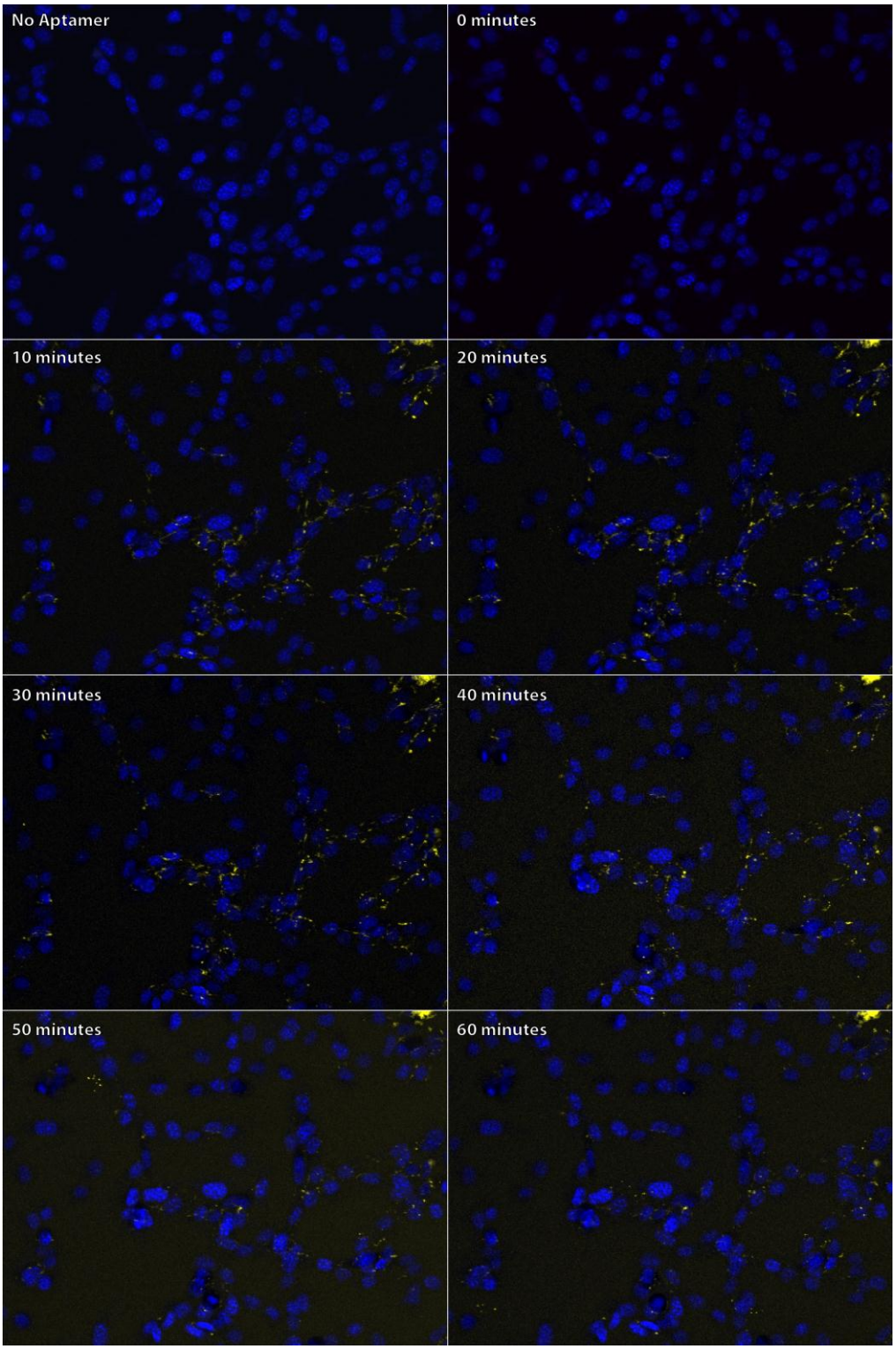

Figure 5. Time-dependent assay with TLS11a aptamer incubation. [100nM] TLS11a added to dish on confocal stage and imaged every ten minutes (no PBS wash step). All images are Z-projections and shown with Hoescht stained nuclei. Micrographs were obtained using a 20x/0.95 numerical aperture water immersion objective at a z-step size of 1.0 µm. Scale bar is equivalent to 20µm.

Quantitative analysis of TLS11a binding was also performed using flow cytometry. Fluorescence intensity histograms of unstained MEAR cells, as well as those labeled with the TD4R negative control aptamer and TLS11a, are shown in Figure 6. TLS11a labeled cells exhibited the highest fluorescence intensity with a median value over 22,000 arbitrary fluorescence units (afu, x-axis) compared to unstained cells with a median of 1,142 afu and control aptamer labeled cells at 4,226 afu. While fluorescent labeling intensity from the TD4R control aptamer was higher than that of unstained cells, the TLS11a aptamer-labeled cell population was still distinct from either negative control population, supporting the affinity of TLS11a aptamer binding to this specific hepatocellular carcinoma cell line. Specificity of the TLS11a aptamer toward non-HCC cell lines was not examined in the current study as it had been previously established in studies by Shangguan et al.[4] Follow-up tissue microarrays from HCC tumors and normal liver tissue are currently being evaluated to further establish specificity of TLS11a for human tissue and tumors (unpublished data).

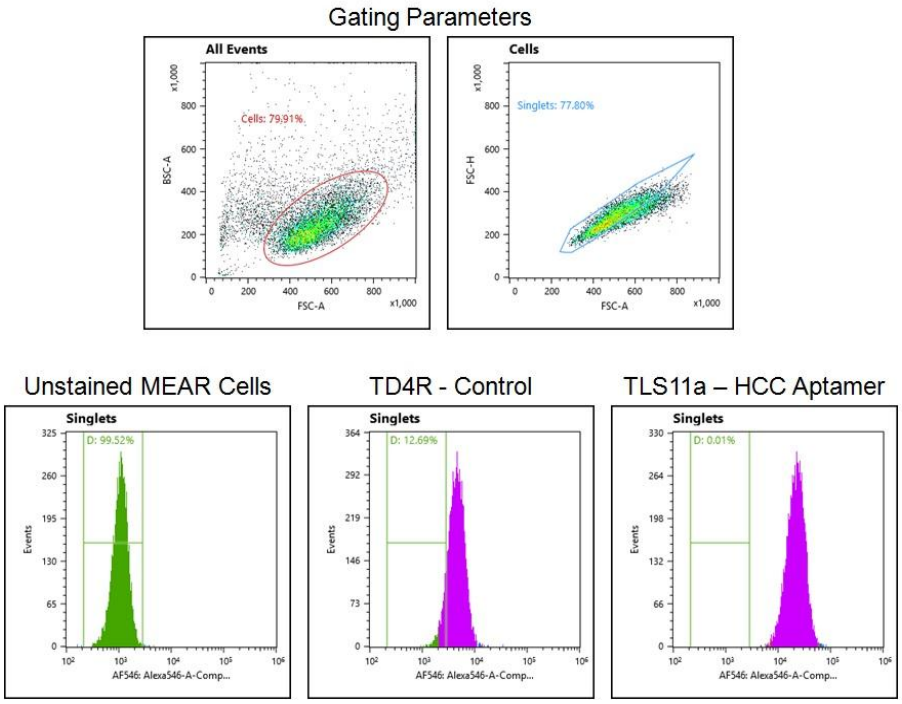

Figure 6. Flow cytometry analysis of HCC cells. The topmost histograms show the gating parameters set for the selection and isolation of cell populations. The lower histograms show the unstained HCC (MEAR) cells compared to cells stained with 5µM concentrations of either the TD4R control aptamer (lower, center) and the TLS11a HCC-specific aptamer (lower, right). The table reflects the median values reported in arbitrary fluorescence units for each population from 10,000 gated events.

Table 2. Mean fluorescent intensity obtained from flow cytometry histograms.

	Mean Fluorescent Intensity (MFI) FL-3
Unstained MEAR cells	1,142
[5 µM] TD4R control	4,226
[5 µM] TLS11a	22,620

3.2 Identification of the proteins recognized by the TLS11a aptamer

In an effort to characterize the TLS11a target protein, the TLS11a/AlexaFluor-546 conjugated aptamer was used in a southwestern blot, such that the DNA aptamer was used to probe proteins following electrophoresis and transfer of proteins extracted from

various cellular components (Figure 7). Prominent bands appeared just over 21 kilodaltons (kDa) in the cell surface protein fraction, the cytosolic hydrophilic protein fraction and in whole cell lysates. Additional bands at roughly 58 kDa and 41 kDa were found in the cytosolic extract and whole cell lysate, respectively. Very faint bands at both these molecular weights could also be seen in the cell surface fraction. No TLS11a-bound protein bands were apparent in the hydrophobic membrane fraction (Figure 7). The absence of aptamer labeling within the hydrophobic membrane protein fraction suggests that the protein recognized by the TLS11a aptamer may not be an integral membrane protein.

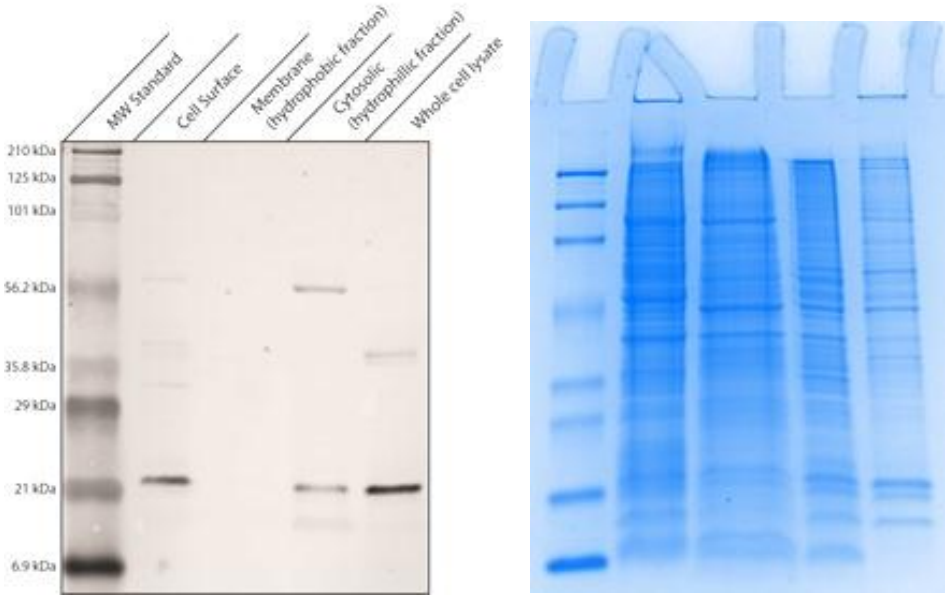

Figure 7. Fluorescent TLS11a/AlexaFluor-546 aptamer-probed western blot and SDS-PAGE gel (8-16% Tris-HCl). Samples included cell surface protein extracts (lane 2), hydrophobic membrane proteins (lane 3), hydrophilic cytosolic proteins (lane 4), and whole cell lysates (lane 5, 10 µg total protein) relative to a broad-range molecular weight standard (lane 1).

3.3 Examination of aptamer-targeted PLGA/PLA-PEG nanoparticles for drug delivery

Since the current evidence supported cell surface binding and uptake of the TLS11a aptamer in HCC cells, its use as a targeting agent for drug delivery was explored with biodegradable PLGA/PLA-PEG polymer nanoparticles. Nanoparticles were prepared by a modified nanoprecipitation technique that combined a mixture of PLGA and PLA-PEG copolymers as described above in the methods section and depicted in (Figure 8). During this process, polymer molecules self-assembled into nanospheres or unevenly shaped nanoparticles as they transitioned from the dissolved state to the solid state consisting of a PLGA/PLA hydrophobic core. In the presence PLGA/PLA-PEG, doxorubicin moved into the hydrophobic interior of the nanoparticle while the COOH-terminal PEG served as a functional group on the particle's surface for conjugation of the

aptamer (Figure 8). Figure 9 shows intensity distributions of particles sizes for doxorubicin-loaded and blank nanoparticles obtained through dynamic light scattering analysis. As show in Figure 9A, nanoparticle size did not change significantly for drug-loaded nanoparticles through the preparation process. The size of blank nanoparticles was not significantly different than that of drug-loaded nanoparticles (Figure 9B). The size polydispersity of the nanoparticles was less than 0.2 in all readings obtained, indicating proper control over the nanoparticle size.

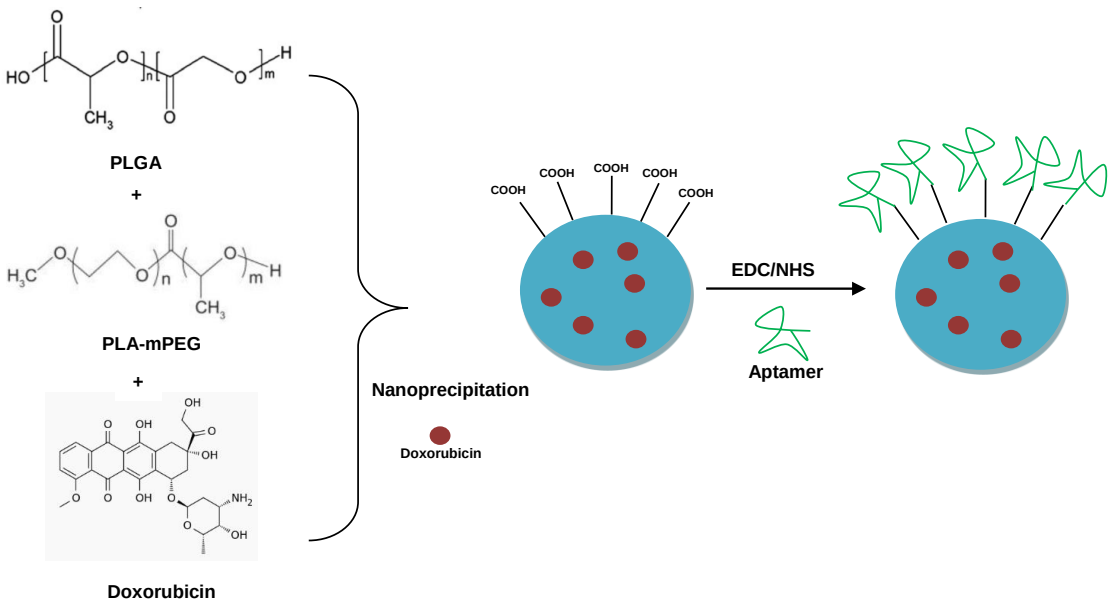

Figure 8. Schematic of PLGA/PLA-PEG polymer nanoparticle synthesis. Copolymer solutions, with/out doxorubicin, were formed by adding the organic polymer solution to an aqueous water solvent; through EDC/NHS chemistry, the aptamer was conjugated to the particles' surface via PEG-COOH functional groups.

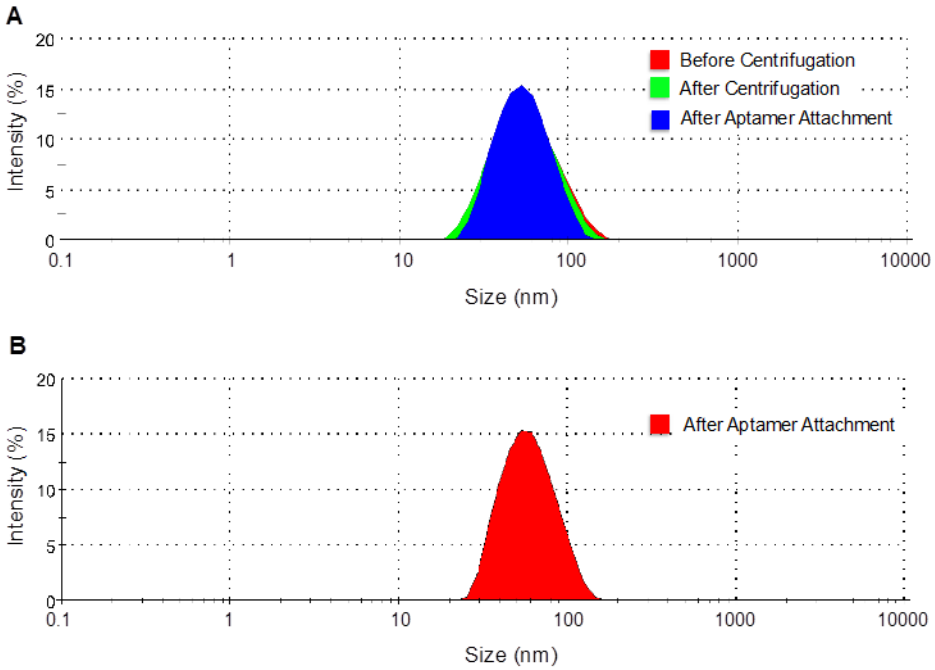

Figure 9. Intensity distribution of nanoparticle sizes obtained through dynamic light scattering analysis. Nanoparticles showed peak sizes in the range of 50 nm, with a size distribution in the order of 30-100 nm. (A) Size distributions of doxorubicin-loaded nanoparticles before initial centrifugation, after two centrifugation cycles, and after aptamer attachment. (B) Size distribution of blank nanoparticles after aptamer attachment.

Following synthesis, the aptamer functionalized nanoparticles carrying the chemotherapeutic drug doxorubicin were used to treat cultured MEAR hepatocellular carcinoma cells, and an MTT assay was used to assess their ability to elicit cell death. Results shown in Figure 10 indicate that both TLS11a aptamer-coated and the uncoated PLGA/PLA-PEG nanoparticles loaded with doxorubicin elicited a marked cytotoxicity greater than that of free doxorubicin alone. This suggests that the polymer nanoparticle delivery vehicle could improve the cellular uptake of doxorubicin; however, there was no added therapeutic benefit from nanoparticles functionalized with the TLS11a aptamer (Figure 10). A reduction in the cell viability (~20%) was seen in the presence of PLGA/PLA-PEG nanoparticles alone (no doxorubicin) demonstrating a low level, albeit,

non-trivial, cytotoxicity from the nanoparticles themselves.

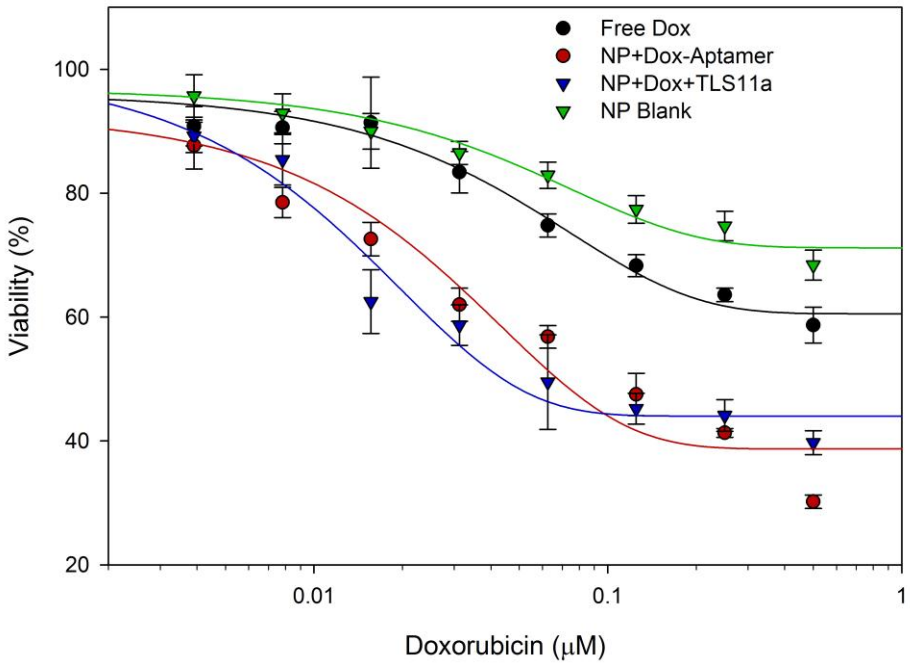

Figure 10. MTT cytotoxicity assay in hepatocellular carcinoma cells. Treatments included solutions containing doxorubicin (black), uncoated PLA-PEG nanoparticles loaded with doxorubicin (red); TLS11a aptamer coated PLA-PEG nanoparticles loaded with doxorubicin (blue) and blank nanoparticles without doxorubicin or aptamer at equivalent nanoparticle concentration (green).

Imaging studies also confirmed that cells treated with the uncoated polymer nanoparticles contained the highest levels of doxorubicin in their nuclei (Figure 11). Doxorubicin has a broad fluorescence excitation and emission spectra; therefore, it was not possible to spectrally separate the aptamer/AlexaFluor-546 signal from the doxorubicin and track their uptake independently (Appendix 1, 2). However, in earlier TLS11a aptamer labeling experiments little to no aptamer signal was found within the nucleus (Figures 3 and 4). Thus, any nuclear fluorescence in cells treated with TLS11a/AlexaFluor-546 aptamer and doxorubicin could reasonably be attributed to the doxorubicin which intercalates DNA in order to elicit cytotoxic effects. MEAR cells

treated with uncoated PLGA/PLA-PEG nanoparticles containing the drug exhibited the highest level of doxorubicin staining in their nuclei followed to a lesser extent by TLS11a aptamer-coated nanoparticles and then free doxorubicin (Figure 11).

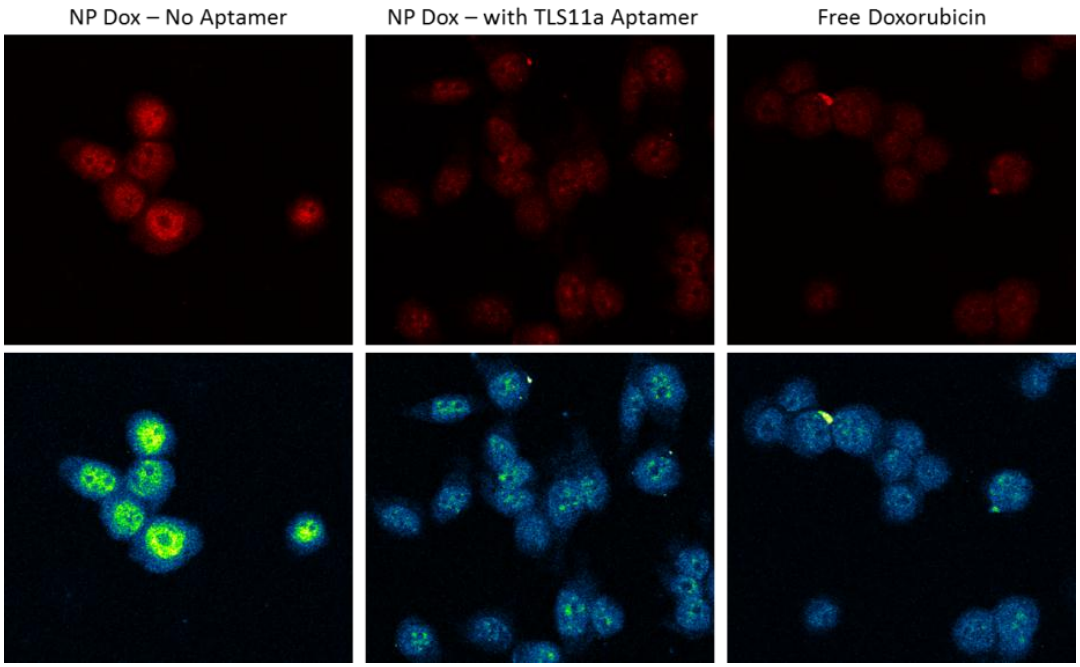

Figure 11. Confocal micrographs of MEAR cells treated with nanoparticle (NP)/drug conjugates. Doxorubicin concentrations were 500 nM (top row). A pseudo-colored heat map LUT was applied to aid the visualization of differences in fluorescence intensity such that low intensity pixels appear blue, while brighter pixels appear green or even yellow (bottom row). Micrographs were obtained using a 60x/1.0 numerical aperture water immersion objective at a z-step size of 1.0 µm.

The release of doxorubicin from PLGA/PLA-PEG nanoparticles was examined over the course of 120 hours versus the diffusion of free doxorubicin in solution at the same concentration. Raw data for the measured doxorubicin absorbance and fluorescence from each time point is summarized in Table 2. The final concentration of doxorubicin was determined by extrapolation from a doxorubicin fluorescence standard curve (Figure 12). Although a standard curve based on doxorubicin absorbance was also drawn, all of

the samples taken from free doxorubicin and the doxorubicin-loaded nanoparticles were below the limit of detection of absorption spectroscopy; therefore, the fluorescence curve was necessary to provide greater sensitivity.

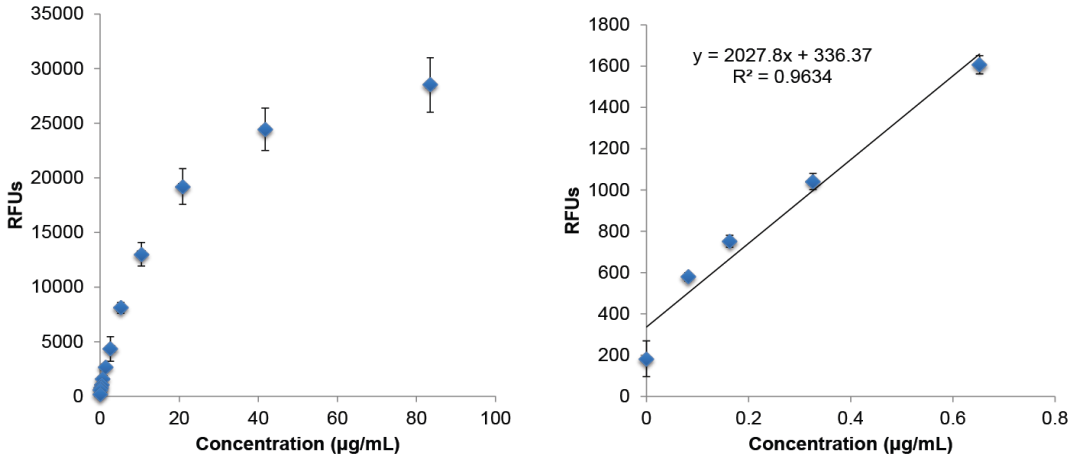

Figure 12. Doxorubicin fluorescence standard curve (left) and linear range at lower concentrations (right).

Preliminary analysis of this data revealed that doxorubicin diffused through the dialysis membrane over time over the course of 120 hours (Figure 13). This rate of diffusion was lower than that expected based on the molecular weight cut-off of the dialysis tubes (8000 Da) versus the molecular weight of doxorubicin (580 Da). Doxorubicin was observed to be released from the nanoparticles at a much lower rate than the doxorubicin solution, as expected (Figure 13). In fact, less than 10% of the drug was eluted within the 120 hours of the release study. Further studies will need to investigate the release of the drug over longer period or times. In addition, studies will need to be performed to determine whether the dialysis method artificially reduced the rate of release of the drug from the nanoparticles.

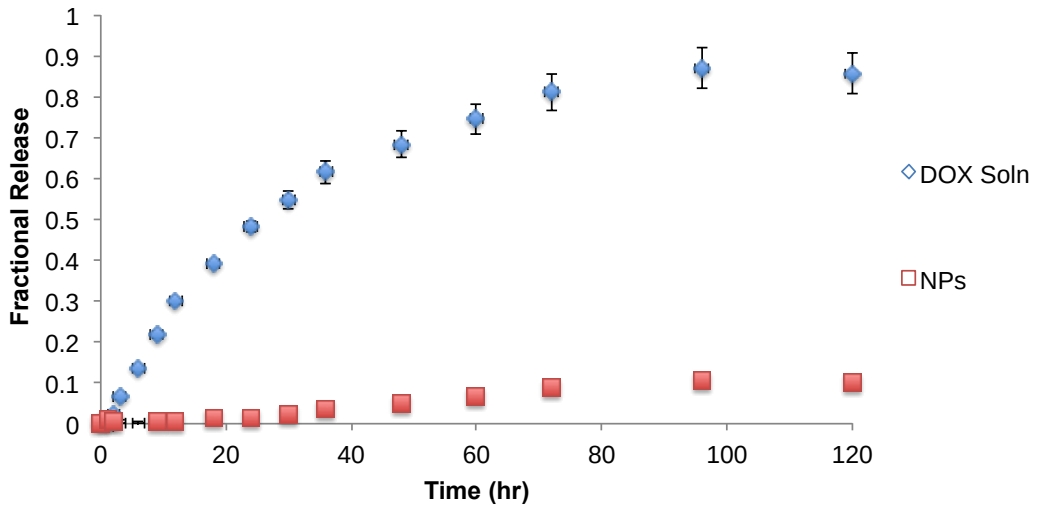

Figure 13. Release profiles for doxorubicin solution and doxorubicin nanoparticles.

Table 3. Doxorubicin UV/VIS absorbance/fluorescence raw data.

	Doxorubicin- NP		Doxorubicin Soln	
Time (hrs.)	Abs (480 nm)	Fluor (590 nm)	Abs (480 nm)	Fluor (590 nm)
1	-0.004	222.9556	0.018	29.28889
2	-0.004	48.62222	-0.003	496.6222
3	-0.003	64.95556	-0.003	833.9556
6	0.002	130.9556	0.007	1270.622
9	0.005	156.6222	0.002	1755.622
12	-0.010	330.2889	-0.003	1670.622
18	0.003	220.2889	-0.001	1516.956
24	-0.003	196.9556	0.002	1983.956
30	-0.004	224.1222	0.000	2650.956
36	-0.002	223.6222	0.000	1880.622
48	0.006	300.9556	0.010	1738.289
60	0.000	398.2889	0.002	1581.622
72	0.008	367.6222	0.000	1457.956
96	-0.002	379.6222	0.002	1395.956
120	-0.002	408.9556	0.000	1544.956

CHAPTER IV

Discussion

In this study, the *in vitro* interactions of a previously reported HCC-specific DNA aptamer[4, 9] was examined using malignant liver cancer cells in order to evaluate its potential utility as a high-affinity targeting agent in applications such as drug delivery. In particular, the aptamer was shown to bind at the cell surface and be taken up via endocytosis-related pathways into acidic compartments, presumably early/late endosomes or lysosomes. Interestingly, the cell surface marker (WGA/AlexaFluor-657) appeared somewhat punctate and clustered in cells labeled with the TLS11a aptamer versus the negative control aptamer where relatively smooth cell outlines were seen with WGA (data not shown). It is possible that some of the WGA was internalized along with the TLS11a aptamer following its binding, or that binding of the TLS11a aptamer to an extracellular protein induced receptor/protein clustering which has been shown to occur in many cell signaling pathways.[15-17] Western blotting results revealed a major aptamer-labeled protein band at 21 kDa in all cell fractions except the hydrophobic membrane proteins, suggesting that the TLS11a target protein is water soluble and not likely to be an integral membrane protein. The presence of corresponding protein bands in the cell surface and the cytoplasmic and whole cell lysate fractions raises several possibilities including the binding of TLS11a to one or more peripheral membrane protein(s) that remained tightly bound to the cell surface during lysis and extraction, or that these extracellular protein could also be found within the cytoplasm following uptake from the cell membrane. The latter scenario is supported by the confocal microscopy localization

studies making the TLS11a aptamer a good candidate for targeted drug delivery where binding and localization are both required for efficient drug delivery.

Unfortunately, the aptamer did not ultimately enhance the cytotoxic effect of doxorubicin when functionalized to a polymer nanoparticle. However, the current study did uphold longstanding evidence for improved drug efficacy when delivered in polymer nanoparticles[11, 14] with increased cytotoxicity of NP-delivered doxorubicin over free doxorubicin. It is possible that the lack of binding by the TLS11a aptamer was due to low concentrations of aptamer on the nanoparticle surface (estimated to be 2.2 nM based upon a fluorescence standard curve) (Appendix, Figure 1). This concentration was far below that needed for either microscopy or flow cytometry. In the concentration-dependent assay, the lowest concentration used was 25 nM, and it was faint, and hard to see. The drastically lower 2.2 nM aptamer estimated on the nanoparticle surface was below the limit of detection based on acquisition settings used for the microscopy study; confocal imaging settings were kept linear to allow for comparison. Optimization of the polymer-to-aptamer conjugation conditions may improve the aptamer loading capacity in future assays. In addition, only a single molecular weight (i.e. length) of PEG polymer was used in the nanoparticle synthesis that could potentially mask or "hide" the aptamer within the flexible polymer shell preventing adequate recognition and binding.[11] This possibility is currently being pursued through the use of various length PEG chains to ensure that the aptamer is freely available for recognition and cell surface binding (data not shown). Taken together, this thesis study provides reasonable support for further examination of the TLS11a as a HCC-specific targeting agent with potential utility in polymer nanoparticle drug delivery for cancer therapeutics, or even diagnostic contrast

enhancement through the inclusion of gold or magnetic nanoparticles for optical or thermal imaging/ablation.

APPENDIX

TLS11a standard curve used to estimate concentration of aptamer on the surface of functionalized nanoparticles. A starting concentration of 100 nM TLS11a was serially diluted across a 96-well plate, and was read for fluorescence intensity, generating the curve below. The nanoparticle-doxorubicin solution was also serially diluted across a 96-well plate, and the fluorescence was read at 560 nm excitation/590 nm emission. Estimation was determined to be 2.2 nM based on this fluorescence data, from the below standard curve.

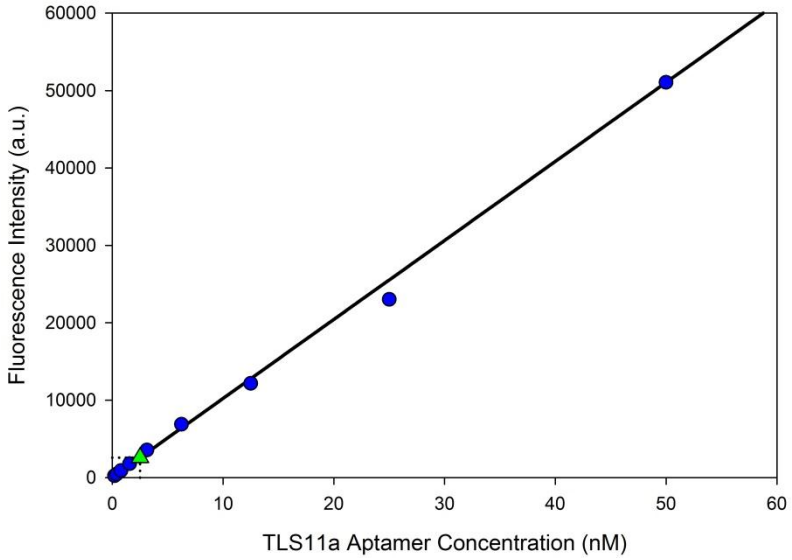

Figure A1. TLS11a aptamer standard curve. Used to estimate the total concentration of aptamer functionalized onto the surface of the PLGA/PLA-PEG nanoparticles. Full range of data points included.

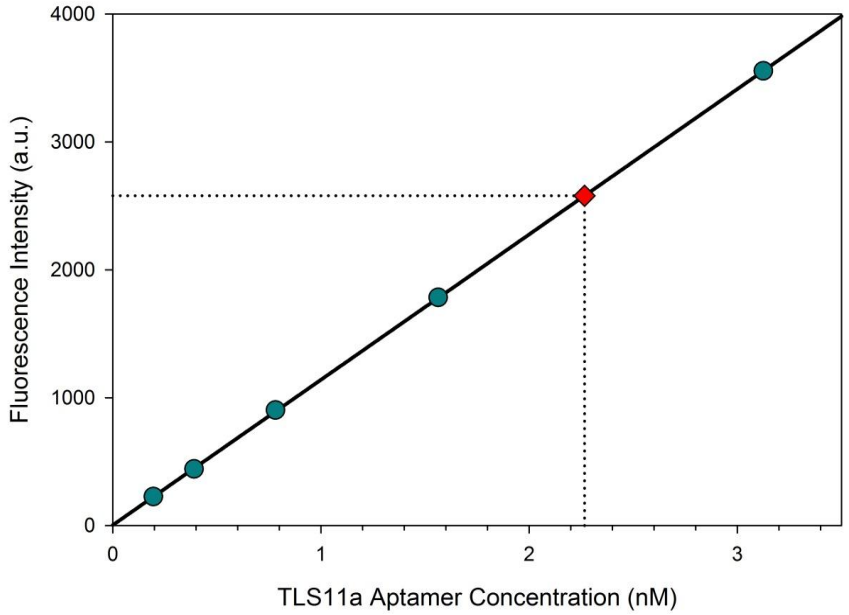

Figure A2. TLS11a aptamer standard curve linear range at lower concentrations. Zoomed in from standard curve in A1. to show the 6 lowest concentration data points. Aptamer concentration on the nanoparticle surface was determined to be 2.2 nM, indicated by the red diamond.

LITERATURE CITED

1. [American Cancer Society: Cancer Facts and Figures 2014] American Cancer Society, Atlanta, GA(2014).

2. S.F. Altekruse, K.A. McGlynn, and M.E. Reichman, "Hepatocellular carcinoma incidence, mortality, and survival trends in the United States from 1975 to 2005," Journal of clinical oncology : official journal of the American Society of Clinical Oncology, 27(9), 1485-91 (2009).

3. K. Khalili, T.K. Kim, H.J. Jang, M.A. Haider, L. Khan, M. Guindi, and M. Sherman, "Optimization of imaging diagnosis of 1-2 cm hepatocellular carcinoma: an analysis of diagnostic performance and resource utilization," J Hepatol, 54(4), 723-8 (2011).

4. D. Shangguan, L. Meng, Z., C. Cao, Z. Xiao, X. Fang, Y. Li, D. Cardona, R.P. Witek, C. Liu, and W. Tan, "Identification of liver cancer-specific aptamers using whole live cells," Anal Chem, 80(3), 721-8 (2008).

5. A.D. Ellington and J.W. Szostak, "In vitro selection of RNA molecules that bind specific ligands," Nature, 346(6287), 818-22 (1990).

6. J. F. Lee, G.M. Stovall, and A.D. Ellington, "Aptamer therapeutics advance," Curr Opin Chem Biol, 10(3), 282-9 (2006).

7. R.E. Wang, Y. Zhang, J. Cai, W. Cai, and T. Gao, "Aptamer-based fluorescent biosensors," Curr Med Chem, 18(27), 4175-84 (2011).

8. E.J. Cho, J.W. Lee, and A.D. Ellington, "Applications of aptamers as sensors," Annu Rev Anal Chem (Palo Alto Calif), 2, 241-64 (2009).

9. L. Meng, L. Yang, X. Zhao, L. Zhang, H. Zhu, C. Liu, and W. Tan, "Targeted delivery of chemotherapy agents using a liver cancer-specific aptamer," PLoS One, 7(4), e33434 (2012).

10. F. Danhier, E. Ansorena, J.M. Silva, R. Coco, A. Le Breton, and V. Préat, "PLGA-based nanoparticles: an overview of biomedical applications," Journal of controlled release : official journal of the Controlled Release Society, 161(2), 505-22 (2012).

11. M. Elsabahy and K.L. Wooley, "Design of polymeric nanoparticles for biomedical delivery applications," Chem Soc Rev, 41(7), 2545-61 (2012)

12. D.M. Bollag, M.D. Rozycki, and S.J. Edelstein, [Protein methods] Wiley-Liss, New York (1996).

13. T. Betancourt, J.D. Byrne, N. Sunaryo, S.W. Crowder, M. Kadapakkam, S. Patel, S. Casciato, and L. Brannon-Peppas, "PEGylation strategies for active targeting of PLA/PLGA nanoparticles," J Biomed Mater Res A, 91(1), 263-76 (2009).

14. T. Betancourt, B. Brown, and L. Brannon-Peppas, "Doxorubicin-loaded PLGA nanoparticles by nanoprecipitation: preparation, characterization and in vitro evaluation," Nanomedicine (Lond), 2(2), 219-32 (2007).

15. V. Horejsi and M. Hrdinka, "Membrane microdomains in immunoreceptor signaling," FEBS Lett, 588(15), 2392-2397 (2014).

16. V.L. Reeves, C.M. Thomas, and E.J. Smart, "Lipid rafts, caveolae and GPI-linked proteins," Adv Exp Med Biol, 729, 3-13 (2012).

17. K.S. George and S. Wu, "Lipid raft: A floating island of death or survival," Toxicol Appl Pharmacol, 259(3), 311-9 (2012).

18. Y.F. Huang, D. Shangguan, H. Liu, J.A. Phillips, X. Zhang, Y. Chen, and W. Tan, "Molecular assembly of an aptamer-drug conjugate for targeted drug delivery to tumor cells," Chembiochem, 10(5), 862-68 (2009).

19. A. Cibiel, N. Quang, K. Gombert, B. Thézé, A. Garofalakis, and F. Ducongé, "From ugly duckling to swan: unexpected identification from cell-SELEX of an anti-annexin A2 aptamer targeting tumors," PLoS ONE, 9(1): e87002 (2014)

20. Y.Y. Lee, K.Q. McKinney, S. Ghosh, D.A. Iannitti, J.B. Martinie, F.R. Caballes, M.W. Russo, W.A. Ahrens, D.H. Lundgren, D.K. Han, H.L. Bonkovsky, and S.I. Hwang, "Subcellular tissue proteomics of hepatocellular carcinoma for molecular signature discovery," J. Proteome Res, 10, 5070-83 (2011).

21. Z. Xiao, D. Shangguan, Z. Cao, X. Fang and W. Tan, "Cell-specific internalization study of an aptamer from whole cell selection," Chem. Eur. J., 14, 1769-75 (2008).

22. M. Ye, J. Hu, M. Peng, J. Liu, J. Liu, H. Liu, X. Zhao and W. Tan, "Generating aptamers by cell-SELEX for applications in molecular medicine," Int. J. Mol. Sci., 13, 3341-53 (2012).

23. K. Sefah, Z. Tang, D. Shangguan, H. Chen, D. Lopez-Colon, Y. Li, P. Parekh, J. Martin, L. Meng, and W. Tan, "Molecular recognition of acute myeloid leukemia usin aptamers," Leukemia, 23(2), 235-44 (2009).

24. J.E. Smith, C.D. Medley, Z. Tang, D. Shangguan, C. Lofton, and W. Tan, "Aptamer-conjugated nanoparticles for the collection and detection of multiple cancer cells," Anal. Chem., 79, 3075-82 (2007).

25. C. Yu, Y. Hu, J. Duan, W. Yuan, C. Wang, H. Xu, and X. Yang," Novel aptamer-nanoparticle bioconjugates enhances delivery of anticancer drug to MUC1-positive cancer cells *in vitro*," PLoS ONE, 6(9): e24077 (2011).

26. M. Brut, A. Trapaidze, A. Estève, A. Bancaud, D. Estève, G. Landa, and M. Djafari-Rouhani, "Bringing aptamers into technologies: impact of spacer terminations," Appl. Phys. Lett., 100, 163702 (2012).

27. G. Zhu, M. Lübbecke, J.G. Walter, F. Stahl, and T. Scheper, "Characterization of optimal aptamer microarray binding chemistry and spacer design," Chem. Eng. Technol., 34(12), 2022-28 (2011).

28. V. Bagalkot, O.C. Farokhzad, R. Langer, and S. Jon, "A aptamer-doxorubicin physical conjugate as a novel targeted drug-delivery platform,"Angew . Chem. Int. Ed. Engl., 45: 8149-52 (2006).

29. L. Zhang, A.F. Radovic-Moreno, F. Alexis, F.X. Gu, P.A. Basto, V. Bagalkot, S. Jon, R.S. Langer, and O.C. Farokhzad, "Co-delivery of hydrophobic and hydrophilic drugs from nanoparticle-aptamer bioconjugates," Chem. Med. Chem., 2:1268-71 (2007).

30. T.R. Pearce, B. Waybrant, and E. Kokkoli, "The role of spacers on the self-assembly of DNA aptamer-amphiphiles into micelles and nanotapes," Chem. Commun., 50:210-12 (2014).

31. Y. Wang, Y. Kuramitsu, M. Takashima, Y. Yokoyama, N. Iizuka, T. Tamesa, I. Sakaida, M. Oka, and K. Nakamura, "Identification of four isoforms of aldolase B down-regulated in hepatocellular carcinoma tissues by means of two-dimensional western blotting," in vivo, 25:881-86 (2011).

32. C.C. Pan, P.C. Chen, S. Tsay, and D.M.T. Ho, "Differential immunoprofiles of hepatocellular carcinoma, renal cell carcinoma, and adrenocortical carcinoma: a systemic immunohistochemical survey using tissue array technique," Appl. Immunohistochem. Mol. Morphol., 13(4):347-52 (2005).